Photoinduced electron transfer between a noble-metal-free [Mo(6)I(8)Cl(6)](2-) cluster and polyoxometalates

Anam Fatima, Yevheniia Smortsova, Clement Falaise, Nathalie Leclerc, Mohamed Haouas, Emmanuel Cadot, Stéphane Cordier, Yann Molard, Thomas Pino, Céline Dablemont, et al.

Photoinduced Electron Transfer Between a Noble-Metal-Free $[Mo_6I_8Cl_6]^{2-}$ Cluster-Based Complex and Polyoxometalates

Anam Fatima,[a] Yevheniia Smortsova,[b] Clément Falaise,*[b] Nathalie Leclerc,[b] Mohamed Haouas,[b] Emmanuel Cadot,[b] Stéphane Cordier,[c] Yann Molard,[c] Thomas Pino,[a] Céline Dablemont,[a] Rachel Méallet,*[a] Karine Steenkeste,*[a] and Minh-Huong Ha-Thi*[a]

Evidence for photoinduced intermolecular electron transfer from the excited state of $[Mo_6I_8Cl_6]^{2-}$ electron-rich cluster-based photosensitizer to polyoxometalates (POMs) is reported. We demonstrated that the global charge density of POMs affects the efficiency of electron transfer. This work paves the way for the rational design of photocatalytic systems using cluster-based complexes as robust noble metal-free photosensitizers.

One of the key challenges toward solar fuel generation is the development of photocatalytic systems involving robust noble-metal-free components.[1] In this context, polyoxometalates (POMs) have been identified as promising earth-abundant metal-based catalysts for light-driven hydrogen evolution reaction when they are associated with sunlight harvesting unit.[2–10] In most of these systems, the photosensitizer corresponds to ruthenium- or iridium-based complexes. Although the electron transfer between the excited state of such complexes and the POM is quite efficient, using abundant element-containing photosensitizers would be highly beneficial to reduce the environmental impact and cost of these photocatalytic devices. Covalent grafting of organic dyes with POMs represents an attractive way to design photoactive POM-based systems.[11–15] Although this approach is elegant, hybrid functionalized POMs exhibit drawbacks such as time-consuming synthetic procedures and in many cases, unavoidable photo-bleaching under prolonged operating irradiation.

The octahedral transition-metal cluster compounds $[M_6X_8Y_6]^{2-}$ consists of six metal centers (Mo^{II} or W^{II}) linked to face-capping (X) and terminal halide ligands (Y).[16,17] These robust inorganic complexes are able to undergo reversible one-electron oxidation[16,18]. Moreover, upon visible-light irradiation they exhibit intense luminescence with high quantum yields and considerably long-lived (µs order) triplet state.[19–23] Based on these striking properties, it was hypothesized in 1983 that $[M_6X_8Y_6]^{2-}$ can behave as photosensitizing units.[24] Although Gray and coworkers observed that the luminescence of $[Mo_6Cl_8Cl_6]^{2-}$ is quenched in the presence of POMs, no spectroscopic signature of the charge separated state has been detected and their lifetime were not characterized.[24] To the best of our knowledge, no experimental proof of photoinduced electron transfer between $[M_6X_8Y_6]^{2-}$ and quenchers has yet been reported.

Herein, we employed nanosecond transient absorption (TA) spectroscopy supported by spectroelectrochemical experiments to reveal unambiguously that the molybdenum halide complex $[Mo_6I_8Cl_6]^{2-}$ is able to transfer one electron to POMs upon visible-light irradiation. The mixed halide $[Mo_6I_8Cl_6]^{2-}$ cluster complex has been selected for this study (Fig. 1A) because it exhibits higher quantum yield than that of the $[Mo_6Cl_8Cl_6]^{2-}$ cluster-based complex previously studied by Gray[24] (47% vs 19%).[16] Moreover, key parameters of the quenching mechanism related to the cluster-POM interplay will be highlighted below by using POMs with various charge densities, nuclearities, and redox potentials, such as the Keggin-type anions $([XW_{12}O_{40}]^{n-}$ with X = P^{5+}, Si^{4+}, B^{3+}, $(2H)^{2+}$ (Fig. 1B) and the Dawson–type anion $[P_2W_{18}O_{62}]^{6-}$ (Fig. 1C).

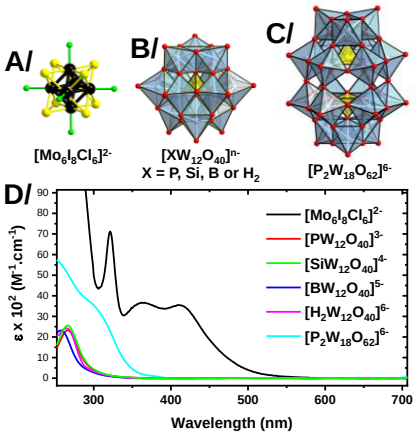

Fig. 1 (A) Structural representation of the molybdenum halide cluster. Black sphere: Mo, yellow sphere: I, green sphere: Cl. (B) and (C) Structural representations of the Keggin-type and Dawson–type POM. (D) Electronic absorption profiles of the cluster and the POMs (as tetrabutylammonium salts) in CH_3CN. Note: The molar extinction coefficients (ε) of POMs are scaled by dividing by a factor of 20.

[a] *ISMO-CNRS UMR 8214, Université Paris-Saclay; Rue André Rivière 91400 Orsay (France). Email : rachel.meallet-renault@universite-paris-saclay.fr; karine.steenkeste@universite-paris-saclay.fr; minh-huong.ha-thi@universite-paris-saclay.fr*

[b] *ILV-CNRS UMR 8180, UVSQ, Université Paris-Saclay; 45 Avenue des Etats Unis, 78035 Versailles Cedex (France). Email : clement.falaise@uvsq.fr*

[c] *Institut des Sciences Chimiques de Rennes, UMR 6226 CNRS, Univ Rennes; Avenue du General Leclerc, 35042 Rennes (France)*

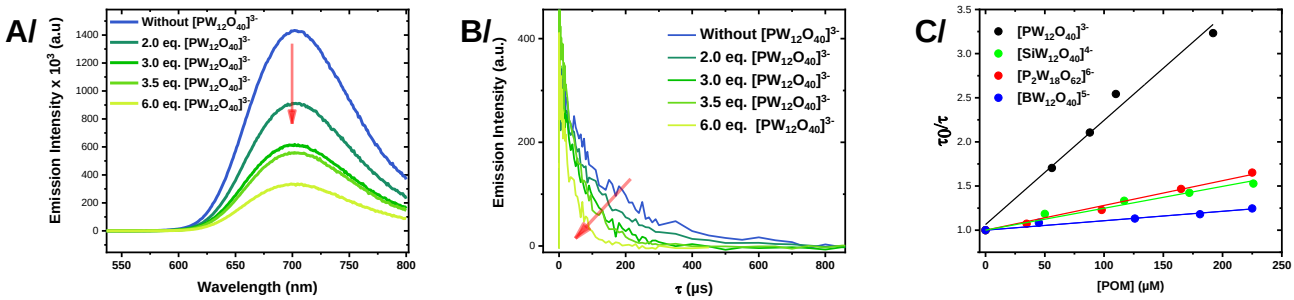

Fig. 2. (A) Steady-state emission spectra and (B) time-resolved emission decays of the $[Mo_6I_8Cl_6]^{2-}$ cluster-based complex (30 µM) in the presence of different concentrations of $[PW_{12}O_{40}]^{3-}$ POM in deaerated CH_3CN and (C) Stern-Volmer plots showing the emission lifetime changes of the cluster in the presence of POMs.

The absorption spectra of the $[Mo_6I_8Cl_6]^{2-}$ complex and that of the POMs in the UV-Visible range are shown in Fig. 1D. The cluster complex exhibits typical intense absorption in near-ultraviolet with a broad low-energy absorption band located at 420 nm (ε = 3 300 $M^{-1}.cm^{-1}$) that corresponds to metal to metal transitions, from bonding to antibonding character.[25] In contrast, the POMs exhibit no or weak absorption in the visible region. Indeed characteristic ligand-to-metal charge-transfer (O→W) bands of tungsten-oxo frameworks are observed in UV region.[26,27] Further, excitation at 420 nm of $[Mo_6I_8Cl_6]^{2-}$ in deaerated CH_3CN gives rise to a broad and intense emission, centered at about 700 nm (Fig. S1, ESI), consistent with that previously reported by Kitamura and coworkers.[16] The emission spectra were also recorded at different temperatures (Fig. S2, ESI), and a slight blue shift was observed at decreasing temperatures as previously reported.[23] Time-resolved emission measurements (Fig. S3, ESI) show that the emission at 700 nm decays with a time constant of 165 ± 10 µs. Measurements in aerated solution reveal a substantial decrease in the excited state lifetime down to 1.6 µs due to oxygen quenching (Fig. S4, ESI), supporting that the detected luminescence arises from the triplet state.[28]

Adding the Keggin anion $[PW_{12}O_{40}]^{3-}$ to argon-saturated solution of $[Mo_6I_8Cl_6]^{2-}$ (30 µM) provokes a strong emission quenching as evidenced by the evolution of the steady-state emission intensities (Fig. 2A) and of the lifetimes (Fig. 2B). For instance, adding about six equivalents of POM reduces the emission intensity of $[Mo_6I_8Cl_6]^{2-}$ by a factor of four. Plotting I_0/I and τ_0/τ as a function of $[PW_{12}O_{40}]^{3-}$ concentration, yields a linear Stern-Volmer (SV) correlation having equivalent slopes (Fig. S5, ESI and Fig. 2C) with a quenching rate constant (k_q) of 9 x 10^7 $M^{-1}.s^{-1}$. The k_q values obtained from the SV plots of the emission lifetimes for the different cluster-POM pairs are given in Table 1. The respective rates obtained from the emission intensities are shown in Table S1 (ESI). A decrease in the emission intensities and lifetimes $[Mo_6I_8Cl_6]^{2-}$ upon adding $[SiW_{12}O_{40}]^{4-}$, $[P_2W_{18}O_{62}]^{6-}$ or $[BW_{12}O_{40}]^{5-}$ anions is also observed, but with a much lower magnitude (Figs. S6, S7 and S8, ESI). The intensity and lifetime SV plots obtained for these three cluster/POM systems (Fig. 2C and S5, ESI) gave lower values of quenching rate constants that are given in Table 1 and Table S1. The linear behavior in both steady-state (I_0/I) and time-resolved (τ_0/τ) measurements shows that the quenching of the excited state is dynamic in nature and suggests that there is a negligible ground state association between the photosensitizer and the quencher.[29] From the comparison of the four studied $[Mo_6I_8Cl_6]^{2-}$/POM tandems, it appears that the values of k_q significantly decreases with the increase of the anionic charge density of the POM unit (q/M = global charge/number of metal atoms, Table 1). The increase of q/M gives rise to different contributions altering the transfer of electron and/or energy between the $[Mo_6I_8Cl_6]^{2-}$ donor and the POM acceptor. The main effect of the q/M may lie within the increase of the electrostatic repulsions between the two inorganic anionic partners of the tandem, therefore limiting *in fine* the approach of the photosensitizer in the close vicinity of the quenching unit. To highlight the key role of q/M on $[Mo_6I_8Cl_6]^{2-}$/POM interplay and in particular, the strong influence of coulombic repulsions within the tandem, we studied the influence of the highest charged Keggin anion of the series $[H_2W_{12}O_{40}]^{6-}$ on the emission lifetime of $[Mo_6I_8Cl_6]^{2-}$. In similar experimental conditions, the quenching process was found negligible and even could not be determined.

Table. 1 Quenching rate constants (k_q) determined from emission lifetime changes for each $[Mo_6I_8Cl_6]^{2-}$/POM tandem.

POMs	Standard potential, V[a]	Charge density (q/M)	$k_q \times 10^7$, $M^{-1}.s^{-1}$
$[PW_{12}O_{40}]^{3-}$	-0.55	0.25	9 ± 2
$[PW_{11}VO_{40}]^{4-}$	-0.33	0.33	2.0 ± 0.3
$[SiW_{11}MoO_{40}]^{4-}$	-0.58	0.33	1.5 ± 0.2
$[SiMo_{12}O_{40}]^{4-}$	-0.68	0.33	1.9 ± 0.3
$[P_2W_{18}O_{62}]^{6-}$	-0.95	0.33	2.0 ± 0.2
$[SiW_{12}O_{40}]^{4-}$	-1.11	0.33	1.1 ± 0.2
$[BW_{12}O_{40}]^{5-}$	-1.45	0.42	0.7 ± 0.1
$[H_2W_{12}O_{40}]^{6-}$	-1.55	0.50	--

[a] The first standard potential of the POM (V *vs* Fc/Fc^+) has been determined by cyclic voltammetry studies in deaerated CH_3CN containing 0.1 M $TBA.PF_6$ (Figs. S9 and S10, ESI).

Besides, we also evaluated the contribution of POM reducibility on the emission quenching of $[Mo_6I_8Cl_6]^{2-}$ using a set of isocharged Keggin-type derivatives exhibiting a first potential covering a range from -330 to -1100 mV *vs* Fc^+/Fc (see Table 1, Figs. S11, S12, S13 and S14, ESI). This study revealed that the k_q value is moderately influenced by the ability of the POM to be reduced. For instance, the k_q value observed for the more reducible POM, $[PW_{11}VO_{40}]^{4-}$, is only twice that observed for $[SiW_{12}O_{40}]^{4-}$, a POM exhibiting first redox potential at -1100 mV. In comparison, a much more pronounced difference of k_q value is observed between $[PW_{12}O_{40}]^{3-}$ and $[SiMo_{12}O_{40}]^{4-}$ while both

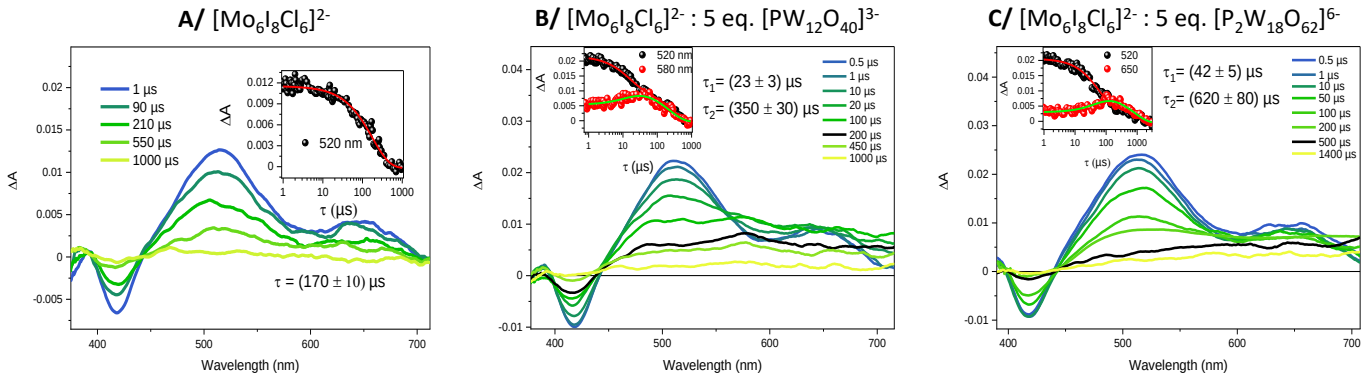

Fig. 3. Transient absorption spectra of (A) cluster $[Mo_6I_8Cl_6]^{2-}$ (30 µM) in the absence of POM and in the presence of 5 equivalents of (B) $[PW_{12}O_{40}]^{3-}$ and (C) $[P_2W_{18}O_{62}]^{6-}$. Measurements have been realized in deaerated CH_3CN, (λ_{exc} = 420 nm). Insets show global fitting of kinetic traces at indicated wavelengths.

exhibit similar reduction potential, reiterating that the *q*/M and, consequently, the coulombic repulsion between the two inorganic units governs mostly the rate of electron transfer.

In addition, it must be pointed out that that the k_q measured for the system $[Mo_6I_8Cl_6]^{2-}/[PW_{12}O_{40}]^{3-}$ in CH_3CN are slightly lower than those reported by Gray *et al.* (70 x 10^7 $M^{-1}.s^{-1}$) for the tandem $[Mo_6Cl_8Cl_6]^{2-}/[PW_{12}O_{40}]^{3-}$ in aqueous solution.[19,24] Although the nature of the molybdenum halide cluster should have an impact on the k_q, the nature of the solvent on the quenching efficiency is also crucial. Actually, the transfer between negatively charged species strongly depends on their mutual coulombic repulsions that are stronger in organic solvent exhibiting low dielectric constant, such as CH_3CN, than in water. To evidence the electron transfer process from the excited state of the octahedral cluster to the POMs, nanosecond TA measurements were performed in deaerated CH_3CN. After excitation of $[Mo_6I_8Cl_6]^{2-}$ at 420 nm, a positive transient absorption band at 520 nm accompanied by a less intense band at around 650 nm was observed, which has been ascribed to the triplet excited state of the cluster (Fig. 3A).[28] The transient absorption spectral features can be satisfactorily fitted with a monoexponential decay of 170 ± 10 µs time constant, which is close to the previously measured emission lifetime.

In the presence of the Keggin-type POM $[PW_{12}O_{40}]^{3-}$, the nanosecond TA spectra (λ_{exc} = 420 nm) of $[Mo_6I_8Cl_6]^{2-}$ revealed a different scenario (Fig. 3B). Until 0.5 µs, the TA spectra show the spectral features of the triplet excited state of $[Mo_6I_8Cl_6]^{2-}$. Then, the signal of the excited state decays and transforms into a new spectroscopic feature absorbing in almost the entire visible range and extending to the near-infrared part (Fig. 3B). This new broad transient absorption band is consistent with the formation of a 1 e- reduced POM, which gives rise to intense intervalence charge transfer (IVCT) band spreading until the NIR domain. The formation of the reduced POM species results from an electron transfer from the cluster to the POM leading to the charge-separated species {oxidized cluster-reduced POM} observed at 200 µs. Beyond 200 µs, the transient absorption signal decays and no change in the spectral shape is observed, reflecting the charge recombination process. Globally, fitting the kinetic traces with a two-exponential model gives two time components of 23 ± 3 and 350 ± 30 µs. The resulting decay-associated difference spectra (DADS) are shown in Fig. S15 (ESI). The short time component of 23 µs is assigned to the decay of the excited $[Mo_6I_8Cl_6]^{2-*}$ concomitant with the rise of charge-separated species, while the latter should correspond to the recombination of the charge-separated pair.

Hypothesis of a photo-induced electron transfer has been further supported by comparison of the broad TA spectroscopic feature (retrieved from the 350 µs DADS) with the sum of the contributions arising from the oxidized mono-anionic $[Mo_6I_8Cl_6]^{-}$ complex and the one electron-reduced POM. The UV-Vis signature of both species has been obtained from separated bulk electrolysis at controlled potential (see details in ESI). The oxidized $[Mo_6I_8Cl_6]^{-}$ molybdenum halide cluster complex gives rise to two principal absorption bands located at about 600 and 800 nm, resulting in a color change from yellow to olive-green (Fig. S16, ESI). Besides, solutions of the one-electron reduced derivative of the $[PW_{12}O_{40}]^{3-}$ ion exhibit a characteristic deep blue color (λ_{abs}^{max} = 750 nm) which is assigned to the *d-d* transitions and IVCT bands (Fig. S17, ESI).[26,30] A good match with TA spectroscopic feature is overall obtained using a linear combination of the respective contributions of the spectro-electrochemical difference spectra of the oxidized cluster and the reduced POM (Fig. 4A). This is consistent with a photoinduced electron transfer from the triplet excited state of $[Mo_6I_8Cl_6]^{2-*}$ to the Keggin-type POM $[PW_{12}O_{40}]^{3-}$. The nanosecond TA experiments have been also carried out with higher charged Keggin-type POMs, $[BW_{12}O_{40}]^{5-}$ and $[H_2W_{12}O_{40}]^{6-}$ (Fig. S18 and S19, ESI). In such systems, a small decrease in the lifetime of the excited state was observed. However, the spectroscopic feature and the dynamics of the charge-separated state could not be detected due to the less efficient electron transfer.

Interestingly, the photoinduced electron transfer was also measured between $[Mo_6I_8Cl_6]^{2-}$ and $[P_2W_{18}O_{62}]^{6-}$, as revealed by the decay of the typical transient absorption signal of the $[Mo_6I_8Cl_6]^{2-*}$ triplet state, concomitant with the rise of a flat, featureless transient absorption signal in the entire visible range associated to the reduced POM (Fig. 3C). This signal is different from that of the system involving the Keggin anion $[PW_{12}O_{40}]^{3-}$ and matches nicely with a combination involving spectra of the oxidized mono-anionic $[Mo_6I_8Cl_6]^{-}$ complex and the one-electron reduced Dawson-type anion (Fig. 4B). Bi-exponential fitting of all the kinetic traces gives time constants of 42 ± 5 and 620 ± 50 µs corresponding to the rise and the decay of the charge-separated state, respectively (Fig. 3C and

Fig. S20, ESI). Hence, the observed $[Mo_6I_8Cl_6]^{2-*}$ excited state has longer lifetime when the tandem partner is a Dawson-type POM as compared to that when the tandem partner is $[PW_{12}O_{40}]^{3-}$. This reflects the less efficient electron transfer consistent with the quenching constant value.

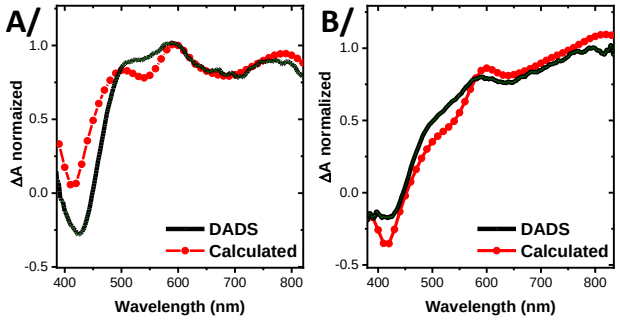

Fig. 4. Comparison of the second decay-associated difference spectrum (DADS) resulted from the global analysis on the TA measurements of the cluster and (A) $[PW_{12}O_{40}]^{3-}$ and (B) $[P_2W_{18}O_{62}]^{6-}$, with the linear combination (calculated) of the spectra of the oxidized cluster $[Mo_6I_8Cl_6]^{-}$ and the one-electron reduced POMs.

In summary, these photophysical investigations demonstrate that the excited state of the noble-metal-free $[Mo_6I_8Cl_6]^{2-}$ cluster-based molybdenum halide can transfer an electron to Keggin- or Dawson-type POMs in CH_3CN. Such donor-acceptor tandems are composed of anionic entities and consequently the rate of electron transfer is dramatically affected by the anionic charge density of the POM unit. The lower the charge density, the higher the electron transfer efficiency, following the series where the charge q per metal atom progressively increases: $[PW_{12}O_{40}]^{3-}$ (0.25) > $[P_2W_{18}O_{62}]^{6-}$ ~ $[SiW_{12}O_{40}]^{4-}$ ~ $[PW_{11}VO_{40}]^{4-}$ ~ $[SiW_{11}MoO_{40}]^{4-}$ ~ $[SiMo_{12}O_{40}]^{4-}$ (0.33) > $[BW_{12}O_{40}]^{5-}$ (0.42) > $[H_2W_{12}O_{40}]^{6-}$ (0.50). This work opens new avenues toward the design of full-inorganic photocatalytic devices by using molybdenum octahedral clusters as noble-metal free inorganic photosensitizers associated to POM as specific catalytic unit efficient for targeted processes such as depolluting, biomass valorization or clean energy generation.[31]

This work was supported by i) Labex Charmmmat (ANR-11-LABX-0039-grant), ii) CLUSPOM-H2 project (ANR-22-CE50-0007-01), iii) Paris-Saclay University, iv) UVSQ and v) CNRS.

Conflicts of interest

There are no conflicts to declare.

Notes and references

1 C. Bie, L. Wang and J. Yu, *Chem*, 2022, **8**, 1567–1574.

2 B. Matt, J. Fize, J. Moussa, H. Amouri, A. Pereira, V. Artero, G. Izzet and A. Proust, *Energy Environ. Sci.*, 2013, **6**, 1504–1508.

3 H. Lv, W. Guo, K. Wu, Z. Chen, J. Bacsa, D. G. Musaev, Y. V. Geletii, S. M. Lauinger, T. Lian and C. L. Hill, *J. Am. Chem. Soc.*, 2014, **136**, 14015–14018.

4 Z.-M. Zhang, T. Zhang, C. Wang, Z. Lin, L.-S. Long and W. Lin, *J. Am. Chem. Soc.*, 2015, **137**, 3197–3200.

5 G. Paille, A. Boulmier, A. Bensaid, M. H. Ha-Thi, T. G. Tran, T. Pino, J. Marrot, E. Riviere, C. H. Hendon, O. Oms, M. Gomez-Mingot, M. Fontecave, C. Mellot-Draznieks, A. Dolbecq and P. Mialane, *Chem. Commun.*, 2019, **55**, 4166–4169.

6 S. Schönweiz, M. Heiland, M. Anjass, T. Jacob, S. Rau and C. Streb, *Chem. Eur. J.*, 2017, **23**, 15370–15376.

7 Y. Luo, S. Maloul, M. Wächtler, A. Winter, U. S. Schubert, C. Streb and B. Dietzek, *Chem. Commun.*, 2020, **56**, 10485–10488.

8 Y. Smortsova, C. Falaise, A. Fatima, M. H. Ha-Thi, R. Méallet-Renault, K. Steenkeste, S. Al-Bacha, T. Chaib, L. Assaud, M. Lepeltier, M. Haouas, N. Leclerc, T. Pino and E. Cadot, *Chem. Eur. J.*, 2021, **27**, 17094–17103.

9 S. Maloul, M. van den Borg, C. Müller, L. Zedler, A. K. Mengele, D. Gaissmaier, T. Jacob, S. Rau, B. Dietzek-Ivanšić and C. Streb, *Chem. Eur. J.*, 2021, **27**, 16846–16852.

10 S. Amthor, S. Knoll, M. Heiland, L. Zedler, C. Li, D. Nauroozi, W. Tobaschus, A. K. Mengele, M. Anjass, U. S. Schubert, B. Dietzek-Ivanšić, S. Rau and C. Streb, *Nat. Chem.*, 2022, **14**, 321–327.

11 F. A. Black, A. Jacquart, G. Toupalas, S. Alves, A. Proust, I. P. Clark, E. A. Gibson and G. Izzet, *Chem. Sci.*, 2018, **9**, 5578–5584.

12 E. Benazzi, J. Karlsson, Y. B. M'Barek, P. Chabera, S. Blanchard, S. Alves, A. Proust, T. Pullerits, G. Izzet and E. A. Gibson, *Inorg. Chem. Front.*, 2021, **8**, 1610–1618.

13 S. Cetindere, S. T. Clausing, M. Anjass, Y. Luo, S. Kupfer, B. Dietzek and C. Streb, *Chem. Eur. J.*, 2021, **27**, 17181–17187.

14 F. Odobel, M. Séverac, Y. Pellegrin, E. Blart, C. Fosse, C. Cannizzo, C. R. Mayer, K. J. Elliott and A. Harriman, *Chem. Eur. J.*, 2009, **15**, 3130–3138.

15 A. Harriman, K. J. Elliott, M. A. H. Alamiry, L. L. Pleux, M. Séverac, Y. Pellegrin, E. Blart, C. Fosse, C. Cannizzo, C. R. Mayer and F. Odobel, *J. Phys. Chem. C*, 2009, **113**, 5834–5842.

16 S. Akagi, S. Fujii and N. Kitamura, *Dalton Trans.*, 2018, **47**, 1131–1139.

17 N. T. K. Nguyen, C. Lebastard, M. Wilmet, N. Dumait, A. Renaud, S. Cordier, N. Ohashi, T. Uchikoshi and F. Grasset, *Sci. Technol. Adv. Mate.*, 2022, **23**, 547–578.

18 N. A. Vorotnikova, Y. A. Vorotnikov, I. N. Novozhilov, M. M. Syrokvashin, V. A. Nadolinny, N. V. Kuratieva, D. M. Benoit, Y. V. Mironov, R. I. Walton, G. J. Clarkson, N. Kitamura, A. J. Sutherland, M. A. Shestopalov and O. A. Efremova, *Inorg. Chem.*, 2018, **57**, 811–820.

19 A. W. Maverick and H. B. Gray, *J. Am. Chem. Soc.*, 1981, **103**, 1298–1300.

20 J. A. Jackson, C. Turro, M. D. Newsham and D. G. Nocera, *J. Phys. Chem.*, 1990, **94**, 4500–4507.

21 H. Miki, T. Ikeyama, Y. Sasaki and T. Azumi, *J. Phys. Chem.*, 1992, **96**, 3236–3239.

22 M. A. Mikhaylov and M. N. Sokolov, *Eur. J. Inorg. Chem.*, 2019, **2019**, 4181–4197.

23 S. Akagi, S. Fujii and N. Kitamura, *J. Phys. Chem. A*, 2018, **122**, 9014–9024.

24 A. W. Maverick, J. S. Najdzionek, D. MacKenzie, D. G. Nocera and H. B. Gray, *J. Am. Chem. Soc.*, 1983, **105**, 1878–1882.

25 R. Ramirez-Tagle and R. Arratia-Pérez, *Chem. Phys. Lett.*, 2008, **460**, 438–441.

26 E. Papaconstantinou, *Chem. Soc. Rev.*, 1989, **18**, 1–31.

27 C. Streb, *Dalton Trans.*, 2012, **41**, 1651–1659.

28 K. Kirakci, P. Kubát, M. Dušek, K. Fejfarová, V. Šícha, J. Mosinger and K. Lang, *Eur. J. Inorg. Chem.*, 2012, **2012**, 3107–3111.

29 B. Valeur and M. N. Berberan-Santos, *Handbook of Fluorescence Spectroscopy and Imaging Fluorescence Applications in Biotechnology and Life Sciences Surface Enhanced Raman Spectroscopy Applied and Industrial Photochemistry*, 2012.

30 G. M. Varga, E. Papaconstantinou and M. T. Pope, *Inorg. Chem.*, 1970, **9**, 662–667.

31 J. J. Walsh, A. M. Bond, R. J. Forster and T. E. Keyes, *Coord. Chem. Rev.*, 2016, **306**, 217–234.